Mixed-Mode Oscillations in a Three Time-Scale Model for the Dopaminergic Neuron

Martin Krupa, Nikola Popović, Nancy Kopell, and Horacio G. Rotstein*
New Mexico State University, Department of Mathematical Sciences,
P.O. Box 30001 Department 3MB, Las Cruces, NM 88003, U.S.A.
Boston University, Center for BioDynamics and Department of Mathematics and Statistics,
111 Cummington Street, Boston, MA 02215, U.S.A. and
New Jersey Institute of Technology, Department of Mathematical Sciences, University Heights, Newark, NJ 07102, U.S.A.
(Dated: August 2, 2007)

Mixed-mode dynamics is a complex type of dynamical behavior that has been observed both numerically and experimentally in numerous prototypical systems in the natural sciences. The compartmental Wilson-Callaway model for the dopaminergic neuron is an example of a system that exhibits a wide variety of mixed-mode patterns upon variation of a control parameter. One characteristic feature of this system is the presence of multiple time-scales. In this article, we study the Wilson-Callaway model from a geometric point of view. We show that the observed mixed-mode dynamics is caused by a slowly varying canard structure. By appropriately transforming the model equations, we reduce them to an underlying three-dimensional canonical form that can be analyzed via a slight adaptation of the approach developed in [1].

PACS numbers: 02.30.Hq,02.30.Mv,87.19.La

Dopamine is a neurotransmitter that is synthesized by so-called dopaminergic neurons in the brain. The dopaminergic neurons of the mammalian brain stem are believed to play a role in movement, cognition, motivation, and reward. Traditional models for this type of neuron [2] have assumed the presence of different ionic mechanisms in the soma and the dendrites. Wilson and Callaway [3] have proposed a coupled oscillator model where these ionic mechanisms are the same throughout the neuron, but where the natural frequency of oscillation varies: The individual oscillators correspond to neuronal compartments, with the compartments representing the soma and proximal dendrites of the neuron having much lower natural frequencies than those representing the more distal regions. More recently, Medvedev and Cisternas [4], as well as Medvedev *et al.* [5], have studied a simplified version of this Wilson-Callaway model. They observed the so-called mixed-mode oscillatory behavior, a complex type of dynamics that is characterized by a mixture of small-amplitude oscillations and large-amplitude (relaxation) excursions. Moreover, Medvedev and Cisternas [4] gave an explanation for this dynamics based on the so-called canard mechanism [6, 7]. In the present article, we extend the analysis of [4], in the sense that we prove how the version of the Wilson-Callaway model analyzed in [4] can be reduced rigorously to a canonical, three-dimensional, three time-scale system formulated in [1]. This reduction is based on geometric singular perturbation theory and geometric desingularization, and allows us to make precise predictions on the mixed-mode dynamics of the original model.

*Electronic address: mkrupa@nmsu.edu,popovic@math.bu.edu,nk@math.bu.edu,rotstein@oak.njit.edu

I. INTRODUCTION

Wilson and Callaway [3] studied N-chains of strongly electrically coupled relaxation oscillators to describe the dynamics of membrane potential and calcium concentration in dopaminergic neurons in the mammalian brain stem. The compartmental model analyzed by Medvedev and Cisternas [4] is slightly simpler, and is given by the following $2N$-dimensional system of equations,

$$\begin{aligned}\varepsilon\frac{dv_i}{dt} &= g_1(v_i)(E_1-v_i)+g_2(u_i)(E_2-v_i)\\ &\quad +\bar{g}_3(E_3-v_i)+d(v_{i+1}-2v_i+v_{i-1}),\end{aligned} \tag{1a}$$

$$\frac{du_i}{dt} = \omega_i\Big(g_1(v_i)(E_1-v_i)-\frac{u_i}{\tau}\Big), \tag{1b}$$

with $i=1,\dots,N$, $v_0\equiv v_1$, and $v_{N+1}\equiv v_N$. (Note that, in contrast to the original Wilson-Callaway equations, (1) is non-dimensionalized, and that the coupling is assumed to be symmetric rather than anisotropic.) The variables v_i and u_i in (1) stand for the voltage and calcium concentration in the ith compartment, respectively. The first three terms in (1a) represent intrinsic currents: A voltage-gated calcium current, a calcium-gated potassium current, and a leak current. The corresponding conductances are given by $g_1(v_i)$, $g_2(u_i)$, and $\bar{g}_3$, respectively, with

$$g_1(v_i)=\frac{\bar{g}_1}{1+\mathrm{e}^{-\frac{v_i-c_1}{c_2}}} \quad\text{and}\quad g_2(u_i)=\frac{\bar{g}_2u_i^4}{u_i^4+c_3^4}. \tag{2}$$

Here, E_j, $\bar{g}_j$, and c_j $(j=1,\dots,3)$ are real constants, cf. [4] and Appendix A. The last term in (1a) models the electrical coupling between adjacent compartments, where the coupling strength d is assumed to be large $(d\gg 1)$. Finally, ε is a small parameter $(0<\varepsilon\ll 1)$.

For the sake of simplicity, we restrict ourselves to the two-compartment case here, *i.e.*, we only consider (1)

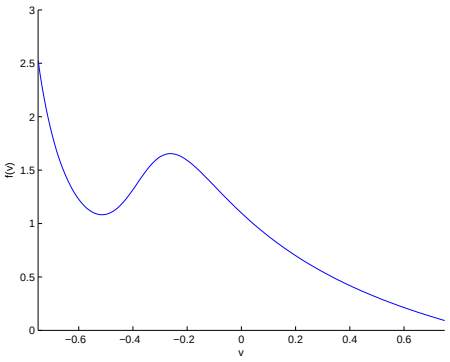

FIG. 1: The function f in (3).

with $N = 2$. Also, following [4], we approximate $g_2(u_i)$ by its linearization about $u_i = 2$ in (1): $g_2(u_i) \approx -au_i+b$. Hence, in sum, we will be concerned with the system of equations

$$\varepsilon\dot{v}_1 = a(E_2 - v_1)\big(f(v_1) - u_1\big) + d(v_2 - v_1), \tag{3a}$$
$$\varepsilon\dot{v}_2 = a(E_2 - v_2)\big(f(v_2) - u_2\big) + d(v_1 - v_2), \tag{3b}$$
$$\dot{u}_1 = \omega_1\Big(g_1(v_1)(E_1 - v_1) - \frac{u_1}{\tau}\Big), \tag{3c}$$
$$\dot{u}_2 = \omega_2\Big(g_1(v_2)(E_1 - v_2) - \frac{u_2}{\tau}\Big), \tag{3d}$$

where the function $f(v_i)$ is defined as

$$f(v_i) = \frac{g_1(v_i)(E_1 - v_i) + \bar{g}_3(E_3 - v_i)}{a(E_2 - v_i)} + \frac{b}{a},$$

cf. [4, p. 339], and the overdot denotes differentiation with respect to t. Note that in the parameter range of interest to us, the graph of f has a qualitatively cubic form, see Figure 1. In particular, we assume that E_j, $\bar{g}_j$, and c_j are chosen such that f is non-negative in the physiologically relevant regime. The values of the parameters in (3) are specified in detail in Appendix A, see also [4].

Clearly, under the above assumptions, (3) is a four-dimensional fast-slow system in standard form, with two fast variables (v_1 and v_2) and two slow variables (u_1 and u_2). One principal finding in [4] is the occurrence of *mixed-mode oscillations (MMOs)* in (3) upon variation of the control parameter τ, which physiologically corresponds to the rate of calcium efflux. In the resulting time series of v_i, small-amplitude oscillations typically alternate with large-amplitude excursions ("spikes"). MMOs are frequently observed in multiple-scale systems of differential equations, such as (1). Consequently, the amplitudes of the mixed-mode patterns found in such systems often vary over several orders of magnitude; see Figures 2 to 4 for an illustration.

Various different mechanisms have been brought forward to explain the emergence of MMOs in fast-slow systems, see, *e.g.*, [1] for a detailed discussion. Recently, a potentially more unified approach has emerged, namely the so-called "(generalized) canard mechanism." This idea, which was formulated by Milik and Szmolyan in the context of the autocatalator [6, 8], has subsequently been extended by a number of authors [7, 9–11]. In fact, it was shown in [4] that the mixed-mode behavior observed in (3) indeed arises via the canard mechanism.

To date, canard-induced MMOs have been studied predominantly in three-dimensional systems with one fast and two slow variables, or in systems that can at least be reduced to this setting; cf. [1, 7–9, 12]. A prototypical system of this type is given as follows:

$$v' = -z + f(v), \tag{4a}$$
$$z' = \varepsilon(v - w), \tag{4b}$$
$$w' = \varepsilon\big(\mu + \phi(v, z, w)\big). \tag{4c}$$

Here, $f(v) = f_2v^2 + f_3v^3 + \mathcal{O}(v^4)$ with f_2 and f_3 real and constant, $\mu > 0$ is a real parameter, and $\phi(v, z, w) = \mathcal{O}(v, z, w)$ is some smooth function.

It is very natural to attempt a reduction of (3) to a system of the form of (4), since the strong diffusive coupling makes v_1 and v_2 essentially indistinguishable. Medvedev and Cisternas [4] perform such a reduction and obtain a hybrid system with two continuous variables, corresponding to v and z in (4), and one discrete variable, which they call the "update constant" K. This reduction is rigorously justified by the results of Medvedev and Kopell [13], who prove the existence of a global strongly attracting three-dimensional invariant manifold $\mathcal{M}$ for (3). In this article, we show that, in suitable coordinates, $\mathcal{M}$ can be interpreted as a globally attracting *slow manifold* of a fast-slow system with singular parameter $\delta = d^{-1}$; consequently, its existence can be deduced from Fenichel theory [14]. Moreover, we introduce a continuous variable w in the process, which is a slowly varying analog of the constant K defined in [4]. An additional coordinate transformation, after restriction of (3) to $\mathcal{M}$, then leads us to a system that is of a form very similar to (4). One major difference between this system and (4) lies in the fact that the variable w is significantly slower than z and, hence, that there are three time-scales present in the former. In [1], we have studied canard-induced MMOs in the family of three-dimensional three time-scale systems given by

$$v' = -z + f_2v^2 + f_3v^3, \tag{5a}$$
$$z' = \varepsilon(v - w), \tag{5b}$$
$$w' = \varepsilon^2(\mu - g_1z). \tag{5c}$$

(Note that v, z, and w are fast, slow, and "super-slow," by (5a), (5b), and (5c), respectively.) We have shown that, due to its three time-scale structure, (5) can be interpreted as a near-integrable system, in the sense that it is a small perturbation of the two-dimensional (v, z)-subsystem in (5). This subsystem, in turn, is a prototypical example of a system that undergoes a so-called canard explosion upon variation of w. Using this observation, we have been able to explain the mixed-mode dynamics of

(5) as arising via "slow passage through a canard explosion." Details on the classical canard phenomenon in the context of two-dimensional fast-slow systems can be found in [15–18].

In the remainder of this article, we show how the three-dimensional, reduced system obtained from (3) after restriction to $\mathcal{M}$ can be fitted into the framework of (5), and how the results obtained in [1] can be adapted to investigate its dynamics. Due to the different powers of ε that will arise in our scaling of (3), the resulting system will differ somewhat from (5). However, we will prove that the same analysis can still be applied. Consequently, our conclusions on the mixed-mode patterns observed in (3) will be in close analogy to those presented in [1], in the context of (5).

To that end, we note that MMO periodic orbits can be characterized by their so-called *Farey sequence* $L_0^{k_0} L_1^{k_1} \dots L_j^{k_j}$, which encodes the number of large-amplitude excursions L_j, respectively the number of small-amplitude oscillations k_j, associated to the given orbit. We will show that for ε sufficiently small, the stable dynamics of (3) is dominated by sequences that are composed of segments of the form 1^k, 1^{k-1}, and 1^{k-2}. Moreover, we will obtain an analytic estimate of the width of the relevant parameter (μ-)interval on which MMOs occur, see equation (40) below; here, $\mu = \tau^{-1}$. Similarly, the stability interval of 1^k-type orbits will turn out to be $\mathcal{O}(\varepsilon^{\frac{3}{4}}(-\ln\varepsilon)^{-\frac{1}{2}})$ wide. Hence, our analysis is an extension of the results of [4]: There, careful numerics was used to show that the equations in (3) display a variety of MMOs with varying τ. However, the analysis in [4] does not provide any explicit results on what Farey sequences can be expected to occur, on what their ordering will be, or on what the size of the corresponding parameter intervals is.

Given that our predictions are based on the leading-order asymptotics of (3), they agree quite well with the numerics, especially in the case considered in [4], where $\omega_1 = 1$ and $\omega_2 = 16$. We discuss the bifurcation structure of (3) in detail only in that case here; however, we will indicate how our results could be extended to the more general case where ω_1 and ω_2 do not necessarily differ by an order of magnitude. Figures 2, 3, and 4 show a sample of the mixed-mode patterns that occur in (3), for different values of ω_2 (16, 4, and 1.5), with $\omega_1 = 1$ fixed.

This article is organized as follows: In Section II, we reduce the four-dimensional system in (3) to a three-dimensional one, via a global reduction to a center manifold $\mathcal{M}$ that can be interpreted as a strongly attracting slow manifold. The resulting system is of the type of (4); such systems are frequently analyzed by reducing their dynamics to the *critical manifold* defined by $z = f(v)$ in (4), and by characterizing the equilibria of the resulting, planar equations [19]. At the end of Section II, we briefly outline this approach in the present context. Then, in Section III, we reformulate the reduced, three-dimensional system on $\mathcal{M}$ to identify its three time-scale structure, and to fit it into the framework of (5). In particular, we indicate how geometric singular perturbation theory can be combined with geometric desingularization to derive asymptotic formulae for the return map induced by the flow of (5). These formulae, in turn, allow us to characterize the mixed-mode dynamics of the original, full system in (3). Notably, the structure of the bifurcation (Farey) sequences observed in (3) is determined by

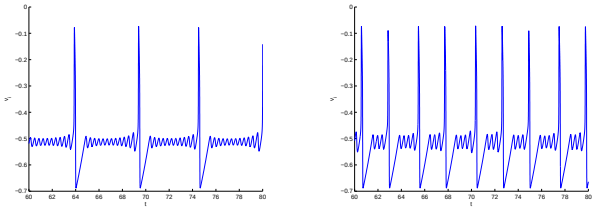

(a) $\tau = 9.7$. (b) $\tau = 9.3$.

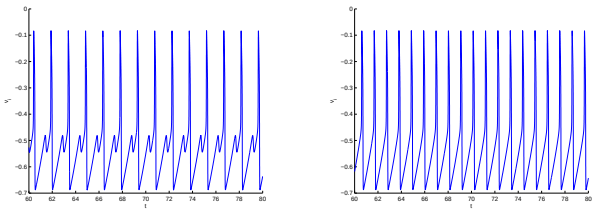

(c) $\tau = 8.9$. (d) $\tau = 8.5$.

FIG. 2: Mixed-mode dynamics for $\omega_2 = 16$ in (3).

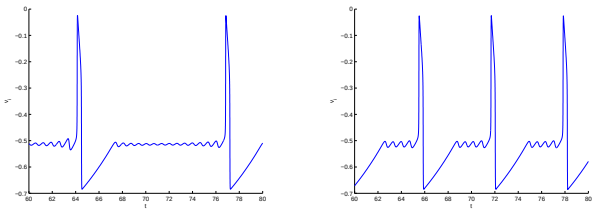

(a) $\tau = 10.0$. (b) $\tau = 9.8$.

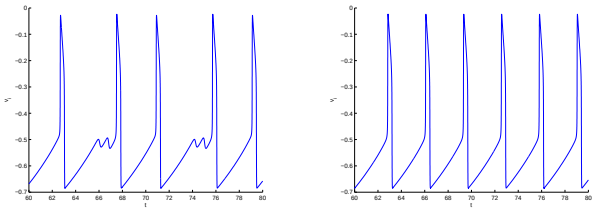

(c) $\tau = 9.6$. (d) $\tau = 9.4$.

FIG. 3: Mixed-mode dynamics for $\omega_2 = 4$ in (3).

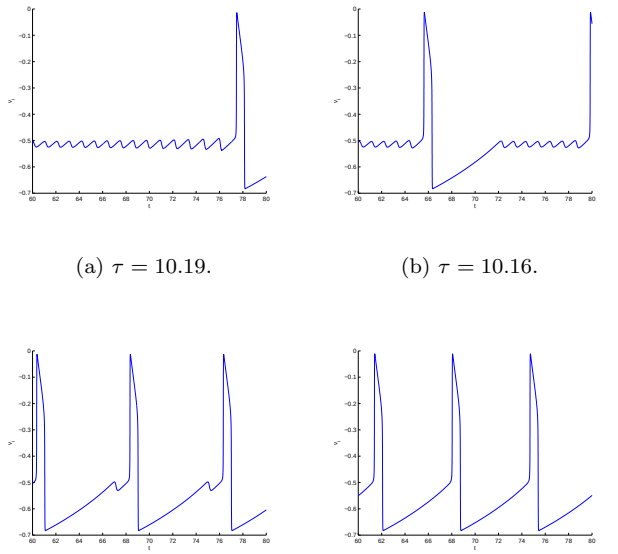

(a) $\tau = 10.19$. (b) $\tau = 10.16$.

(c) $\tau = 10.13$. (d) $\tau = 10.1$.

FIG. 4: Mixed-mode dynamics for $\omega_2 = 1.5$ in (3).

the presence of so-called *secondary canards*; an in-depth discussion of these notions can be found in [1]. Finally, in Section IV, we summarize and discuss our results, and we illustrate them numerically.

II. A GLOBAL CENTER MANIFOLD REDUCTION

The results of [4] strongly indicate the existence of a global invariant (center) manifold $\mathcal{M}$ for (3) in the limit of strong coupling. This conclusion is based on the following property of (3): For $d > 0$ sufficiently large, *i.e.*, for $\delta := d^{-1} \ll 1$, there exists some $t_0 > 0$ such that

$$v_2(t) - v_1(t) = \mathcal{O}(\delta) \quad \text{for all } t \geq t_0 \tag{6}$$

as long as the corresponding trajectories remain uniformly bounded. A proof of (6) is given in [13, Theorem 7.1] in the simplified setting of chains of coupled FitzHugh-Nagumo oscillators.

The idea that a global center manifold reduction for (3) is possible will allow us to eliminate one of the fast (v_i-)variables from the problem. More specifically, we postulate that $\mathcal{M}$ is defined by the condition

$$v_2 = v_1 + \delta\tilde{\vartheta}(v_1, u_1, u_2, \varepsilon, \delta), \tag{7}$$

where $\tilde{\vartheta}$ is a smooth function, possibly depending on ε and δ, but bounded as $\varepsilon, \delta \to 0$; see [4, Equation (3.9)]. We will prove that this postulate follows by standard Fenichel theory [14] once suitable coordinates have been introduced in (3). The manifold $\mathcal{M}$ will contain the relevant dynamics of (3), in the sense that it will be a global attractor for the corresponding flow.

2.1. The center manifold as a slow manifold

We first show that there is an additional (super-fast) time-scale in (3) that is associated with the relaxation of the system to its global, three-dimensional center manifold $\mathcal{M}$ [20]. The resulting fast-slow structure, which has to be superimposed on the scale decomposition induced by the small parameter ε, will allow us to describe $\mathcal{M}$ as a slow manifold after appropriately reformulating (3). (This contrasts with the approach in [4, 13], where (6) was established via a hierarchy of detailed asymptotic estimates.)

We begin by rewriting (3) in terms of the fast time $\tilde{t} = \frac{t}{\varepsilon}$:

$$v_1' = a(E_2 - v_1)\big(f(v_1) - u_1\big) + d(v_2 - v_1), \tag{8a}$$
$$v_2' = a(E_2 - v_2)\big(f(v_2) - u_2\big) + d(v_1 - v_2), \tag{8b}$$
$$u_1' = \varepsilon\omega_1\Big(g_1(v_1)(E_1 - v_1) - \frac{u_1}{\tau}\Big), \tag{8c}$$
$$u_2' = \varepsilon\omega_2\Big(g_1(v_2)(E_1 - v_2) - \frac{u_2}{\tau}\Big). \tag{8d}$$

Given that $\mathcal{M}$ must, to leading order, be given by $v_2 = v_1$, we introduce the sum and difference variables

$$x = \frac{v_1 - v_2}{2} \quad \text{and} \quad y = \frac{v_1 + v_2}{2} \tag{9}$$

in (8).

Now, let

$$\begin{aligned} h_1(x, y, u_1, u_2) = \frac{1}{2}\Big(&a\big(E_2 - (x + y)\big)\big(f(x + y) - u_1\big) \\ &- a\big(E_2 - (-x + y)\big)\big(f(-x + y) - u_2\big)\Big), \\ h_2(x, y, u_1, u_2) = \frac{1}{2}\Big(&a\big(E_2 - (x + y)\big)\big(f(x + y) - u_1\big) \\ &+ a\big(E_2 - (-x + y)\big)\big(f(-x + y) - u_2\big)\Big); \end{aligned}$$

then, (8a) and (8b) become

$$\begin{aligned} x' &= -2dx + h_1(x, y, u_1, u_2), \\ y' &= h_2(x, y, u_1, u_2). \end{aligned}$$

Dividing the first equation by d, we obtain

$$\begin{aligned} \delta x' &= -2x + \delta h_1(x, y, u_1, u_2), \\ y' &= h_2(x, y, u_1, u_2), \end{aligned} \tag{10}$$

which is a singularly perturbed system in its slow formulation, with singular parameter δ. The corresponding critical manifold $\mathcal{M}_0$ obtained for $\delta = 0$ is given by $\{x = 0\}$. Note that $\mathcal{M}_0$ is clearly normally hyperbolic; hence, standard geometric singular perturbation (Fenichel) theory is applicable [14].

Taking into account (8c) and (8d), the fast system corresponding to (10) is given by

$$\begin{aligned}\dot{x} &= -2x + \delta h_1(x, y, u_1, u_2),\\ \dot{y} &= \delta h_2(x, y, u_1, u_2),\\ \dot{u}_1 &= \varepsilon\delta\omega_1\Big(g_1(v_1)(E_1 - v_1) - \frac{u_1}{\tau}\Big),\\ \dot{u}_2 &= \varepsilon\delta\omega_2\Big(g_1(v_2)(E_1 - v_2) - \frac{u_2}{\tau}\Big),\end{aligned} \tag{11}$$

where the overdot now denotes differentiation with respect to the new fast time. With x defined as in (9), an approximation for $\tilde{\vartheta}$ can be obtained by writing the slow manifold for (11) in the form

$$x = \delta\hat{\vartheta}(y, u_1, u_2, \varepsilon, \delta) \tag{12}$$

and by computing the asymptotic expansion of $\hat{\vartheta}$ in powers of δ:

$$\hat{\vartheta}(y, u_1, u_2, \varepsilon, \delta) = \sum_{j=0}^{\infty} \delta^j \hat{\vartheta}_j(y, u_1, u_2, \varepsilon). \tag{13}$$

To that end, we first differentiate (12) with respect to time and then make use of (8) and (11) to derive the invariance condition

$$\begin{aligned}-2\hat{\vartheta} + h_1(\delta\hat{\vartheta}, y, u_1, u_2) &= \delta\Big[\frac{\partial\hat{\vartheta}}{\partial y} h_2(\delta\hat{\vartheta}, y, u_1, u_2)\\ &+ \frac{\partial\hat{\vartheta}}{\partial u_1}\varepsilon\omega_1\Big(g_1(\delta\hat{\vartheta} + y)\big(E_1 - (\delta\hat{\vartheta} + y)\big) - \frac{u_1}{\tau}\Big)\\ &+ \frac{\partial\hat{\vartheta}}{\partial u_2}\varepsilon\omega_2\Big(g_1(-\delta\hat{\vartheta} + y)\big(E_1 - (-\delta\hat{\vartheta} + y)\big) - \frac{u_2}{\tau}\Big)\Big].\end{aligned} \tag{14}$$

We now substitute (13) in (14), equate like powers of δ, and solve the resulting equations inductively. To leading order, we find

$$\hat{\vartheta}_0 = \frac{1}{2}\big[h_1(0, y, u_1, u_2)\big]_0,$$

where $[h_j]_k$ denotes the terms of order k in the Taylor expansion of h_j in δ around $x = 0$. It now follows from

$$f(\pm\delta\hat{\vartheta} + y) = f(y) \pm \delta\hat{\vartheta} f'(y) + \mathcal{O}(\delta^2)$$

that $[h_1]_0 = \frac{1}{2}a(E_2 - y)(f(y) - u_1 - f(y) + u_2)$, and, hence, that

$$\hat{\vartheta}_0(y, u_1, u_2, \varepsilon) = -\frac{a}{4}(E_2 - y)(u_1 - u_2). \tag{15}$$

Note that to lowest order, there is no ε-dependence in $\hat{\vartheta}$.

***Remark* 1.** One can proceed in a similar manner to determine the first-order correction $\hat{\vartheta}_1$ in (13). As it turns out, $\hat{\vartheta}_1$ does depend on ε, in contrast to $\hat{\vartheta}_0$. In fact, we expect that all subsequent terms in (13) will also be ε-dependent.

In terms of the original variables v_1 and v_2, we find

$$\begin{aligned}v_2 &= v_1 + \delta\frac{a}{2}(E_2 - v_1)(u_1 - u_2) + \mathcal{O}(\delta^2)\\ &= v_1 + \delta\tilde{\vartheta}_0(v_1, u_1, u_2, \varepsilon) + \mathcal{O}(\delta^2)\end{aligned} \tag{16}$$

from (15), with $\tilde{\vartheta}_0(v_1, u_1, u_2, \varepsilon) = \tilde{\vartheta}(v_1, u_1, u_2, \varepsilon, 0)$. As we will show, it suffices to consider this lowest-order approximation for $\tilde{\vartheta}$ in order to reproduce qualitatively the results of [4].

2.2. A preliminary transformation of (3)

We now modify the equations in (3) as follows: First, we define the new variable

$$w = \frac{\omega_2 u_1 - \omega_1 u_2}{\omega_1 + \omega_2};$$

then, we use the Ansatz in (7); finally, we note that, given (7) and

$$\begin{aligned}&g_1\big(v_1 + \delta\tilde{\vartheta}(v_1, u_1, u_2, \varepsilon, \delta)\big)\\ &\qquad = g_1(v_1) + \delta\tilde{\vartheta}(v_1, u_1, u_2, \varepsilon, 0) g_1'(v_1) + \mathcal{O}(\delta^2),\end{aligned}$$

we obtain

$$\begin{aligned}g_1(v_1)(E_1 - v_1) - g_1(v_2)(E_1 - v_2) &= \delta\tilde{\vartheta}(v_1, u_1, u_2, \varepsilon, 0)\\ &\times \big(g_1(v_1) - g_1'(v_1)(E_1 - v_1)\big) + \mathcal{O}(\delta^2).\end{aligned}$$

With these definitions, (3) becomes

$$\begin{aligned}\varepsilon\dot{v}_1 &= a(E_2 - v_1)\big(f(v_1) - u_1\big) + \vartheta(v_1, u_1, w, \varepsilon, \delta),\\ \dot{u}_1 &= \omega_1\Big(g_1(v_1)(E_1 - v_1) - \frac{u_1}{\tau}\Big),\\ \dot{w} &= \frac{\omega_1\omega_2}{\omega_1 + \omega_2}\delta\Big(\vartheta(v_1, u_1, w, \varepsilon, 0)\\ &\qquad \times \big(g_1(v_1) - g_1'(v_1)(E_1 - v_1)\big) + \mathcal{O}(\delta)\Big)\\ &\qquad - \frac{\omega_2}{(\omega_1 + \omega_2)\tau}\big((\omega_1 - \omega_2)u_1 + (\omega_1 + \omega_2)w\big),\end{aligned} \tag{17}$$

where $\vartheta(v_1, u_1, w, \varepsilon, \delta) = \tilde{\vartheta}(v_1, u_1, u_2, \varepsilon, \delta)$ now. In particular, by making use of the definition of w to eliminate u_2 from (16), we find

$$\begin{aligned}&\vartheta(v_1, u_1, w, \varepsilon, 0)\\ &\qquad = \frac{a}{2\omega_1}(E_2 - v_1)\big((\omega_1 - \omega_2)u_1 + (\omega_1 + \omega_2)w\big)\end{aligned} \tag{18}$$

for the leading-order asymptotics of ϑ.

***Remark* 2.** The introduction of w is motivated by the definition of the constant K in [4]. In fact, our analysis shows that w is a continuous analog of K. Moreover, it is obvious that ϑ has to depend on w, see (18), whereas [4, Equation (3.9)] suggests no such dependence on K.

Substituting (18) in (17), we find that for $\delta = 0$,

$$\varepsilon\dot{v}_1 = a(E_2 - v_1)\Big(f(v_1) + \frac{\omega_1+\omega_2}{2\omega_1}(-u_1 + w)\Big), \quad (19a)$$

$$\dot{u}_1 = \omega_1\Big(g_1(v_1)(E_1 - v_1) - \frac{u_1}{\tau}\Big), \quad (19b)$$

$$\dot{w} = -\frac{\omega_2}{(\omega_1+\omega_2)\tau}\big((\omega_1-\omega_2)u_1 + (\omega_1+\omega_2)w\big). \quad (19c)$$

The equations in (19) are of the type considered in [19], with one fast variable v_1 and two slow variables u_1 and w. Now, we note that the prefactor $a(E_2 - v_1)$ in (19a) is always non-zero on physiological grounds. (More precisely, $a(E_2 - v_1) > 0$, since we are only interested in $E_2 - v_1 < 0$ and since $a < 0$ by assumption, cf. Appendix A.) Hence, it follows that the corresponding critical manifold for (19), obtained in the singular limit of $\varepsilon = 0$, is defined by

$$\Big(f(v_1) + \frac{\omega_1+\omega_2}{2\omega_1}(-u_1 + w)\Big) = 0.$$

Alternatively, this manifold, which we denote by $\mathcal{S}_0$, can be represented as

$$u_1 = \phi(v_1, w) := \frac{\omega_1}{\bar{\omega}}f(v_1) + w, \quad (20)$$

where $\bar{\omega} = \frac{\omega_1+\omega_2}{2}$ is the arithmetic mean of ω_1 and ω_2. Note that (20) is identical to the expression obtained in [4, Equation (3.13)], with K there replaced by the new variable w here. Hence, w can be considered a continuous analog of K that varies on the slow time-scales defined by δ and τ^{-1}.

Finally, in analogy to [4, Equation (3.7)], we can define the so-called "coupling current" between the two compartments in (17) by

$$\tilde{c}(v_1, u_1, u_2, \varepsilon, \delta) = -\frac{\tilde{\vartheta}(v_1, u_1, u_2, \varepsilon, \delta)}{a(E_2 - v_1)}.$$

Here, we have used $d(v_2 - v_1) = \tilde{\vartheta}$, cf. (7). In particular, for $\delta \to 0$, it follows from (20) after some calculation that

$$c(v_1, u_1, w, \varepsilon, 0) := \tilde{c}(v_1, u_1, u_2, \varepsilon, 0) = \frac{\omega_1-\omega_2}{\omega_1+\omega_2}f(v_1) + w$$

to leading order, in analogy to [4, Equation (3.12)].

To simplify the subsequent analysis, we introduce a new variable z in (19), with

$$z = \frac{\bar{\omega}}{\omega_1}(u - w).$$

(Here and in the following, we omit the subscripts 1 in (v_1, u_1) for the sake of readability.) In terms of (v, z, w), (19) is transformed to

$$\varepsilon\dot{v} = a(E_2 - v)\big(f(v) - z\big), \quad (21a)$$

$$\dot{z} = \bar{\omega}g_1(v)(E_1 - v) - \frac{\omega_1^2+\omega_2^2}{\tau(\omega_1+\omega_2)}z - \frac{\omega_1-\omega_2}{2\tau}w, \quad (21b)$$

$$\dot{w} = -\frac{\omega_1\omega_2}{\tau\bar{\omega}}\Big(\frac{\omega_1-\omega_2}{\omega_1+\omega_2}z + w\Big). \quad (21c)$$

These are the equations that will be studied now. In particular, in the context of (21), the critical manifold $\mathcal{S}_0$ is defined by the constraint $f(v) - z = 0$.

2.3. The reduced equations for (21)

In this subsection, we briefly outline how the so-called *reduced equations* [10, 19] for (21) can be derived. These equations are obtained in the singular limit of $\varepsilon = 0$ in (21) and can be interpreted as a planar system of differential equations with phase space given by the critical manifold $\mathcal{S}_0$:

$$0 = f(v) - z, \quad (22a)$$

$$\dot{z} = \bar{\omega}g_1(v)(E_1 - v) - \frac{\omega_1^2+\omega_2^2}{\tau(\omega_1+\omega_2)}z - \frac{\omega_1-\omega_2}{2\tau}w, \quad (22b)$$

$$\dot{w} = -\frac{\omega_1\omega_2}{\tau\bar{\omega}}\Big(\frac{\omega_1-\omega_2}{\omega_1+\omega_2}z + w\Big). \quad (22c)$$

(Here, we recall that $a(E_2 - v) > 0$ in (21) and, hence, that this prefactor can be canceled for $\varepsilon = 0$.) The motivation for studying the reduced system (22) is to locate so-called *folded equilibria*, which are essential for classifying the canard dynamics of (21).

Now, recall that the function f in (22a) has a qualitatively cubic form, cf. again Figure 1. Consequently, $f'(v) = 0$ vanishes for exactly two values of v, which we denote by v^+ and v^-; numerically, one finds $v^+ \approx -0.2618$ and $v^- \approx -0.5141$ for the parameter values specified in Appendix A. We will denote the two *fold lines* where $v = v^\pm$ is constant by $\ell^\pm$, respectively, and we observe that $\ell^\pm$ are lines of equilibria for (22).

Next, we note that $f'(v) < 0$ for $v < v^-$ and $v > v^+$, as well as that $f'(v) > 0$ for $v^- < v < v^+$. Hence, for (v, z, w) in some closed and bounded subset of $\mathbb{R}^3$, the critical manifold $\mathcal{S}_0$ will consist of two attracting sheets, $\mathcal{S}_0^{a-} : \{v < v^-\}$ and $\mathcal{S}_0^{a+} : \{v > v^+\}$, and a repelling one, $\mathcal{S}_0^r : \{v^- < v < v^+\}$, with the respective boundaries given by $\ell^\pm$. By standard singular perturbation (Fenichel) theory [14], these sheets will perturb, smoothly in ε for $\varepsilon > 0$ sufficiently small, to sheets $\mathcal{S}_\varepsilon^{a-}$, $\mathcal{S}_\varepsilon^{a+}$, and $\mathcal{S}_\varepsilon^r$ of the slow manifold $\mathcal{S}_\varepsilon$ that are unique up to exponentially small terms in ε. (In other words, away from $\ell^\pm$, the reduced dynamics of (22) is a good approximation for the full dynamics of (21).)

Finally, we discuss the dynamics of (22) near the fold lines $\ell^\pm$. A typical point on the fold is characterized by the property that solutions reaching it in forward or backward time cannot be continued as solutions of (22). For the dynamics of (21), this implies that solutions passing near such points have to leave the slow-evolution regime close to $\mathcal{S}_0$ and undergo relaxation; in other words, they leave the vicinity of the fold under the fast flow of (21). So-called folded equilibria, on the other hand, are special, in that an entire family of solutions of (22) can in fact pass through the fold at these points, see, *e.g.*, [19]. In the following subsection, we will briefly discuss folded

equilibria in the context of (21). A more detailed discussion can be found in the article by Jalics *et al.* [21] which will also be included in the present issue.

2.4. Folded equilibria for (21)

To find folded equilibria for (21), we follow the procedure outlined in [10]. Since we are projecting (22) onto $\mathcal{S}_0$, or, equivalently, onto the (v,w)-plane, we begin by eliminating any z-dependence from the equations. Making use of the constraint in (22a), we substitute $z = f(v)$ and $\dot{z} = f'(v)\dot{v}$ in (22) to obtain

$$\begin{aligned} f'(v)\dot{v} &= \bar{\omega} g_1(v)(E_1 - v) \\ &\quad - \frac{1}{4\tau\bar{\omega}}\big(2(\omega_1^2+\omega_2^2)f(v) + (\omega_1^2-\omega_2^2)w\big), \end{aligned} \tag{23a}$$

$$\dot{w} = -\frac{\omega_1\omega_2}{\tau\bar{\omega}}\Big(\frac{\omega_1-\omega_2}{\omega_1+\omega_2}f(v) + w\Big). \tag{23b}$$

Next, we perform a trajectory-dependent time rescaling which introduces the factor $-f'(v)$ in the right-hand sides of (23). Canceling this factor in (23a), we find

$$\begin{aligned} \dot{v} &= -\bar{\omega}(E_1 - v)g_1(v) \\ &\quad + \frac{1}{4\tau\bar{\omega}}\big(2(\omega_1^2+\omega_2^2)f(v) + (\omega_1^2-\omega_2^2)w\big), \end{aligned} \tag{24a}$$

$$\dot{w} = \frac{\omega_1\omega_2}{\tau\bar{\omega}}f'(v)\Big(\frac{\omega_1-\omega_2}{\omega_1+\omega_2}f(v) + w\Big), \tag{24b}$$

where the overdot now denotes differentiation with respect to the new rescaled time. The expression in brackets in (24b) is precisely the coupling current c [4].

***Remark* 3.** Similar results can be obtained from the full (four-dimensional) fast-slow system (3) via the alternative approach outlined in [7].

Equilibria of (24) now correspond to folded equilibria of the original equations (21). These equilibria are classified according to their character as equilibrium points of the rescaled planar system (24), *i.e.*, according to the local dynamics of the reduced flow near the fold. (Note, however, that folded equilibria are generally not equilibria for the original reduced equations in (23).) Here, we are especially interested in *folded nodes* and *folded saddle-nodes*; see [19] for details. Typically, this type of folded equilibria occurs in problems which exhibit mixed-mode dynamics. More precisely, the small-oscillation component of MMO time series frequently arises in a region that limits on a folded (saddle-)node [9, 10]. In fact, as we will show below, this is precisely the scenario that gives rise to the mixed-mode patterns observed in (3).

The equilibria of (24), which we denote by (v^*, w^*), are determined as follows: Once v^* is known, w^* is obtained by setting the right-hand side in (24a) equal to zero, which gives

$$w^* = \frac{\omega_1+\omega_2}{\omega_1-\omega_2}\tau(E_1 - v^*)g_1(v^*) - 2\frac{\omega_1^2+\omega_2^2}{\omega_1^2-\omega_2^2}f(v^*). \tag{25}$$

Note that, in contrast to v^*, the value of w^* *does* depend on τ. To characterize the corresponding equilibria, we linearize (24) about (v^*, w^*), making use of $f'(v^*) = 0$:

$$\begin{bmatrix} -\bar{\omega}\big((E_1 - v^*)g_1'(v^*) - g_1(v^*)\big) & \frac{\omega_1^2-\omega_2^2}{4\tau\bar{\omega}} \\ \frac{2\omega_1\omega_2}{(\omega_1-\omega_2)\tau}f''(v^*)\big(\tau(E_1-v^*)g_1(v^*) - f(v^*)\big) & 0 \end{bmatrix}. \tag{26}$$

Given the analysis in [4], it seems reasonable to assume that the canard phenomenon should occur near ℓ^-. In fact, as we will show below, ℓ^+ contains only jump points, *i.e.*, points at which trajectories must leave $\mathcal{S}_0$ under the fast flow, at least in the parameter range relevant to us.

Hence, let P^- now denote the folded equilibrium of (24) with $v^* = v^-$, where the corresponding w^*-value w^- is determined from (25). Motivated by the analysis in [4], we will consider $w^- = w^-(\tau)$ for varying τ, with the values of the remaining parameters in (25) as specified in Appendix A. Note that $P^- \in \ell^-$ is a local minimum of f, see Figure 1, which implies in particular $f''(v^-) > 0$.

Now, denote by $[\ldots]_{ij}$ the (i,j)th entry in (26), and note that $[\ldots]_{12} < 0$ always holds, whereas the sign of $[\ldots]_{21}$ depends on the sign of $\tau(E_1 - v^*)g_1(v^*) - f(v^*)$, since the prefactor is negative for $v^* = v^-$. We are interested in the cases when P^- is a node or a saddle-node. The transition between these two occurs when $[\ldots]_{21}$ changes sign, *i.e.*, when one of the eigenvalues of (26) goes through zero and P^- undergoes a saddle-node bifurcation. From (26), one finds that the critical value τ_{sn} of τ for which $[\ldots]_{21} = 0$ is given by

$$\tau_{\mathrm{sn}} = \frac{f(v^-)}{(E_1 - v^-)g_1(v^-)}. \tag{27}$$

(A closer inspection of (26) reveals that P^- is a folded saddle-node of type II [7], since the eigendirection corresponding to the zero eigenvalue is not tangent to ℓ^- for $\tau = \tau_{\mathrm{sn}}$.) For the parameters as given in Appendix A, the approximate value of τ_{sn} is 10.2119, while $w^-(\tau_{\mathrm{sn}}) \approx 0.9547$, in agreement with the findings in [4].

Finally, we need to determine whether there exist folded equilibria on the "upper" fold line ℓ^+ when (24) is close to saddle-node bifurcation, *i.e.*, for $\tau \approx \tau_{\mathrm{sn}}$. Numerically, one finds from (25) that $w^*(\tau) \approx -0.8913\tau + 3.3346$ on ℓ^+ and, hence, that $w^*(\tau) < 0$ in the τ-regime of interest to us. Since u_1 and u_2 are non-negative by assumption, it follows from the definition of w and from our choice of ω_1 and ω_2 that negative w-values would correspond to unphysiological values of u_i. Hence, for our purposes, the line ℓ^+ can be regarded as consisting entirely of jump points; in other words, it plays no role in our analysis.

III. REFORMULATION OF (21)

In this section, we show that the mixed-mode dynamics of (3) can be explained by a canard phenomenon which

arises through the saddle-node bifurcation at $\tau = \tau_{\rm sn}$ in (21): For the parameter values chosen as in Appendix A, the equations in (21) can be interpreted as a small perturbation of the almost integrable two-dimensional (v, z)-subsystem (21a),(21b), with w taking the role of a slowly varying parameter. The emergence of small-amplitude oscillations is then triggered by a "slow passage through a canard explosion" around $P^- \in \ell^-$. The necessary analysis is based on an adaptation of the more general results of [1] to the present context and can only be outlined here; the reader is referred to the upcoming article [1] for details.

3.1. A local formulation for (21)

To fit the equations in (21) into a framework that is better suited for a comparison with the results of [1], we first perform a sequence of normalizing transformations about the point $P^- = (v^-, z^-, w^-)$, where v^- and w^- are defined as in Section II **2.4** and $z^- = f(v^-)$. Recall that $\mu = \tau^{-1}$, and define $\gamma := g_1(v^-)(E_1 - v^-)$. Note that γ is an artificial, new parameter that will prove useful for the subsequent analysis. Next, we perform the change of variables $v \mapsto v^- + v$, $z \mapsto f(v^-) + z$, and $w \mapsto w^- + w$ to translate P^- into the origin. (As we will see, this translation is an important step in the transformation of (21) into a system that is similar to the canonical form derived in [1].)

With these definitions, one obtains from (21), after some elementary but lengthy algebraic manipulations, the following system of equations:

$$v' = a(E_2 - v^- - v)\big(- z + f_2 v^2 + f_3 v^3 + \mathcal{O}(v^4)\big), \tag{28a}$$

$$z' = \varepsilon\Big(\bar\omega\big(g_{11} v + \mathcal{O}(v^2)\big) - \frac{\omega_1^2 + \omega_2^2}{\omega_1 + \omega_2}\mu z - \frac{\omega_1 - \omega_2}{2}\mu w\Big), \tag{28b}$$

$$\begin{aligned} w' = \varepsilon\Big(&- 2\frac{\omega_1\omega_2}{\omega_1 - \omega_2}\gamma + 2\frac{\omega_1\omega_2}{\omega_1 - \omega_2} f(v^-)\mu \\ &- 2\frac{\omega_1\omega_2}{\omega_1 + \omega_2}\mu w - 2\omega_1\omega_2\frac{\omega_1 - \omega_2}{(\omega_1 + \omega_2)^2}\mu z\Big). \end{aligned} \tag{28c}$$

Here, f_2 and f_3 are the coefficients of the Taylor expansion of f about v^-, $g_{11} = g_1'(v^-)(E_1 - v^-) - g_1(v^-)$, and the prime again denotes differentiation with respect to the fast time $\tilde t$.

An important characteristic of the compartmental Wilson-Callaway model [3] is the presence of multiple time-scales due to the significantly different intrinsic frequencies of adjacent neuronal compartments. Namely, it is assumed that $\omega_i \ll \omega_{i+1}$ for $i \geq 1$, cf. Section I. In the context of (28), this assumption simplifies to $\omega_1 \ll \omega_2$; in particular, Medvedev and Cisternas [4] take $\omega_1 = 1$ and $\omega_2 = 16$, see also Appendix A. An additional scale in (28) is determined by the fact that μ and γ are $\mathcal{O}(\sqrt{\varepsilon})$ in the regime of interest to us: Note that $\varepsilon = 0.013$, again by Appendix A, and recall that $\mu \approx \tau_{\rm sn}^{-1} \approx 0.1$; similarly, one can show numerically that $\gamma \approx 0.1$. To reflect these observations, we introduce the following rescaling in (28):

$$\omega_2 = \frac{\tilde\omega_2}{\sqrt{\varepsilon}}, \quad \gamma = \sqrt{\varepsilon}\tilde\gamma, \quad \mu = \sqrt{\varepsilon}\tilde\mu. \tag{29}$$

Finally, to reduce (28) as closely as possible to the canonical system (5) formulated in [1], we rescale w via

$$w = \frac{2}{\tilde\omega_2\tilde\mu}\frac{\tilde w}{\sqrt{\varepsilon}}.$$

As a result, the equations in (28) are transformed as follows:

$$\begin{aligned} v' = {} & a(E_2 - v^- - v) \\ & \times \big(- z + f_2 v^2 + f_3 v^3 + \mathcal{O}(v^4)\big), \end{aligned} \tag{30a}$$

$$z' = \sqrt{\varepsilon}\Big(\frac{\tilde\omega_2}{2} g_{11} v + \tilde w + \mathcal{O}(\sqrt{\varepsilon}v, \sqrt{\varepsilon}z, \sqrt{\varepsilon}\tilde w, v^2)\Big), \tag{30b}$$

$$\begin{aligned} \tilde w' = {} & \varepsilon^{\frac{3}{2}}\big[\sqrt{\varepsilon}\nu(\tilde\mu, \sqrt{\varepsilon}) - \big(2\omega_1 + \mathcal{O}(\sqrt{\varepsilon})\big)\tilde\mu\tilde w \\ & + \sqrt{\varepsilon}\big(\omega_1\tilde\omega_2 + \mathcal{O}(\sqrt{\varepsilon})\big)\tilde\mu^2 z\big], \end{aligned} \tag{30c}$$

where

$$\nu(\tilde\mu, \sqrt{\varepsilon}) = \omega_1\tilde\omega_2\tilde\mu\big(\tilde\gamma - f(v^-)\tilde\mu\big) + \mathcal{O}(\sqrt{\varepsilon}). \tag{31}$$

Note that (30) is a fast-slow system with three distinct time-scales, and that the structure of the equations is similar to that of (5); the major difference lies in the powers of ε that occur, and in their respective ratios. Nevertheless, as we will show below, the approach developed in [1] can again be applied in the analysis of (30). In particular, the two-dimensional (v, z)-subsystem in (30), which is to leading order given by

$$\begin{aligned} v' &= a(E_2 - v^- - v)(-z + f_2 v^2 + f_3 v^3), \\ z' &= \sqrt{\varepsilon}\Big(\frac{\tilde\omega_2}{2} g_{11} v + \tilde w\Big), \end{aligned} \tag{32}$$

with $\tilde w$ treated as a parameter, is a system that undergoes a classical canard explosion at $\tilde w = 0$ [22].

***Remark* 4.** The introduction of $\tilde w$ makes the connection between (30) and (5) immediate; more precisely, (30b) shows that $\tilde w$, and not w, is the slowly varying "canard parameter," see [1] for details.

3.2. Dynamics of (30) close to ℓ^-

To analyze (30) in a neighborhood of the fold line ℓ^-, we need to rescale the equations once again; this is due to the fact that the scale separation in (30) breaks down near ℓ^-, which implies a loss of normal hyperbolicity [14]. The required rescaling is analogous to that in [1, Equation (2.2)], except for the fact that the corresponding powers of ε must be adjusted to the context of (30):

$$v = \varepsilon^{\frac{1}{4}}\bar v, \quad z = \sqrt{\varepsilon}\bar z, \quad \tilde w = \varepsilon^{\frac{1}{4}}\bar w. \tag{33}$$

(Note that (33) is one specific realization of the more general technique of geometric desingularization, or blow-up, that has been applied successfully in numerous situations where hyperbolicity is lost, see, *e.g.*, [16, 22] for details.)

We now carry out (33) and subsequently cancel a factor of $\varepsilon^{\frac{1}{4}}$ from the right-hand sides of the resulting equations, which corresponds to a rescaling of time, to obtain the following system:

$$\begin{aligned}\bar{v}' &= a(E_2 - v^-)\Big[-\bar{z} + f_2\bar{v}^2 + \varepsilon^{\frac{1}{4}}\Big(f_3 - \frac{f_2}{E_2 - v^-}\Big)\bar{v}^3 \\ &\quad + \varepsilon^{\frac{1}{4}}\frac{1}{E_2 - v^-}\bar{v}\bar{z} + \mathcal{O}(\varepsilon^{\frac{1}{2}}\bar{v}^4)\Big],\end{aligned} \tag{34a}$$

$$\bar{z}' = \frac{\tilde{\omega}_2}{2}g_{11}\bar{v} + \bar{w} + \mathcal{O}(\sqrt{\varepsilon}\bar{v}, \varepsilon^{\frac{3}{4}}\bar{z}, \sqrt{\varepsilon}\bar{w}, \varepsilon^{\frac{1}{4}}\bar{v}^2), \tag{34b}$$

$$\begin{aligned}\bar{w}' &= \varepsilon\big[\sqrt{\varepsilon}\nu(\tilde{\mu}, \sqrt{\varepsilon}) - \varepsilon^{\frac{1}{4}}\big(2\omega_1 + \mathcal{O}(\sqrt{\varepsilon})\big)\tilde{\mu}\bar{w} \\ &\quad + \varepsilon\big(\omega_1\tilde{\omega}_2 + \mathcal{O}(\sqrt{\varepsilon})\big)\tilde{\mu}^2\bar{z}\big].\end{aligned} \tag{34c}$$

As in [1], the effect of (33) on (30) is to eliminate the scale separation between v and z, and to unlock the near-integrable structure of the dynamics in the fold region. More precisely, for $\varepsilon = 0 = \bar{w}$, the $(\bar{v}, \bar{z})$-subsystem

$$\begin{aligned}\bar{v}' &= a(E_2 - v^-)(-\bar{z} + f_2\bar{v}^2), \\ \bar{z}' &= \frac{\tilde{\omega}_2}{2}g_{11}\bar{v}\end{aligned} \tag{35}$$

of (34) is integrable, with a constant of motion H that can be found in analogy to [1, Equation (2.5)]:

$$\begin{aligned}H(\bar{v}, \bar{z}) = \frac{\tilde{\omega}_2}{4}g_{11}\mathrm{e}^{-4\frac{a(E_2 - v^-)}{\tilde{\omega}_2 g_{11}}f_2\bar{z}} \\ \times\left(-\bar{v}^2 + \frac{1}{f_2}\bar{z} + \frac{\tilde{\omega}_2 g_{11}}{4a(E_2 - v^-)f_2^2}\right).\end{aligned}$$

Correspondingly, the orbits of (35) are determined by the level curves of H, *i.e.*, by $H(\bar{v}, \bar{z}) = h$ constant.

We will require the following notation; the reader is referred to [1, Section 2.2] for details. For $\varepsilon > 0$ and a given h-value, let $\bar{\gamma}_\varepsilon^h(t) = (\bar{v}, \bar{z}, \bar{w})(t)$ denote the corresponding solution to (34), and let $\overline{\Delta}_-$ be the section for the flow of (34) defined by $\bar{v} = 0$ and $\bar{z} < 0$. (Here and in the following, barred quantities denote objects after the rescaling in (33), *i.e.*, in the new $(\bar{v}, \bar{z}, \bar{w})$-coordinates.) Note that for $h \in (-h_0, h_0)$, with $h_0 > 0$ sufficiently small, $\bar{\gamma}_\varepsilon^h$ can be parametrized by h, in the sense that to any such h there corresponds precisely one value of $\bar{z}$ in $\overline{\Delta}_-$.

For $\varepsilon = 0 = \bar{w}$ and h fixed, denote by $\bar{\gamma}_0^h(t)$ the solution of the singular equations in (35) with $H(\bar{v}, \bar{z}) = h$, and note that the corresponding orbit will be a closed level curve of H for $h > 0$, respectively an open one for $h < 0$; typical such curves are illustrated in Figure 5(a). Now, given $h > 0$, let the time parametrization of $\bar{\gamma}_0^h$ be chosen such that $\bar{\gamma}_0^h(-T^h) = \bar{\gamma}_0^h(T^h)$ lies in $\overline{\Delta}_-$ for some $T^h > 0$, and note that one can show

$$T^h = \frac{2}{\sqrt{a(E_2 - v^-)\tilde{\omega}_2 g_{11}}}\sqrt{-\ln h} + \mathcal{O}(1), \tag{36}$$

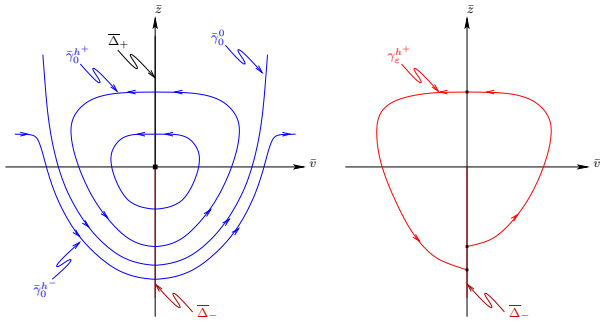

(a) $\varepsilon = 0$. (b) $\varepsilon > 0$.

FIG. 5: Dynamics of the rescaled system (34).

in analogy to [1, Appendix A]. The associated (closed) orbits of (35) are singular templates for the small-amplitude component of the mixed-mode patterns observed in (30); cf. again Figure 5(a). For $\varepsilon > 0$, these orbits will "break up" and perturb as indicated in Figure 5(b).

Finally, the parabolic orbit of $\bar{\gamma}_0^0(t) = (\bar{v}_0^0, \bar{z}_0^0)(t)$, which is the solution to (35) obtained for $h = 0$, corresponds precisely to the so-called *strong canard* in the limit as $\varepsilon \to 0$. This strong canard, which will be denoted by Γ_ε^0, is a trajectory that lies in the transverse intersection of the continuation of $\mathcal{S}_\varepsilon^{a-}$ and $\mathcal{S}_\varepsilon^r$ into the fold region under the flow of (30), thereby connecting these two sheets of the slow manifold $\mathcal{S}_\varepsilon$. (As shown in [1], Γ_ε^0 is well-defined in the context of (30) once $\mathcal{S}_\varepsilon$ is chosen, uniquely up to exponentially small terms in ε.) The strong canard is important insofar as it separates the small-amplitude regime in (30) from the relaxation regime; in other words, it "organizes" [1] the mixed-mode dynamics of (30).

3.3. The global return mechanism

We now discuss the global return mechanism for (28), which describes the dynamics away from the fold lines $\ell^\pm$, without making specific assumptions on the intrinsic frequencies ω_1 and ω_2. We will only assume that $\omega_2 > \omega_1$ for the moment; the assumption that $\omega_1 \ll \omega_2$, which has been used extensively in our analysis so far, is not required for the following argumentation.

First, we claim that the transition from steady-state to oscillatory behavior occurs for $\mu = \frac{\gamma}{f(v^-)}$ in (28). To that end, we note that (28c) has an equilibrium which is stable, as well as that the corresponding equilibrium of the full system (28) loses stability through a Hopf bifurcation as $\gamma - \mu f(v^-)$ passes through 0 (or, alternatively, as τ passes through τ_{sn}, cf. (27)).

Next, we derive an asymptotic formula for the global return and discuss its dependence on $\omega_2 - \omega_1$ as well as the implications for the mixed-mode dynamics of (28).

Due to the presence of a μ-factor, the terms

$$-\frac{\omega_1^2+\omega_2^2}{\omega_1+\omega_2}\mu z \qquad \text{and} \qquad -\frac{\omega_1-\omega_2}{2}\mu w$$

in (28b) are small compared to $\bar{\omega}(g_{11}v+\mathcal{O}(v^2))$ and can hence be neglected. Using a similar argument as in [1, Section 2.5], we then obtain a first-order equation which describes the global return to leading order:

$$\frac{dw}{dv} = \Psi_0(v)w + \Psi_1(v), \tag{37}$$

with

$$\Psi_0(v) = -\frac{\omega_1\omega_2}{\bar{\omega}^2}\mu\frac{f'(v^-+v)}{g(v)}$$

and

$$\Psi_1(v) = 2\frac{\omega_1\omega_2}{\bar{\omega}}\frac{f'(v^-+v)}{g(v)}\Big(\frac{-\gamma+f(v^-)\mu}{\omega_1-\omega_2} - \frac{\omega_1-\omega_2}{(\omega_1+\omega_2)^2}\mu\big(f(v^-+v)-f(v^-)\big)\Big),$$

where g is defined as $g(v)=(E_1-v)(g_1(v^-+v)-g_1(v^-))$. The exact solution of (37), which allows us to express w as a function of v, is given by

$$w(v) = \exp\Big[\int_{v^*}^{v}\Psi_0(\sigma)\,d\sigma\Big]w^* + \int_{v^*}^{v}\exp\Big[-\int_{v^*}^{\sigma}\Psi_0(\sigma')\,d\sigma'\Big]\Psi_1(\sigma)\,d\sigma; \tag{38}$$

here, $w^*=w(v^*)$. For the sake of simplicity, we only consider the leading-order approximation in μ of (38). Since we want to assume that we have passed the onset of oscillation, *i.e.*, that $\gamma-\mu f(v^-)>0$, it follows that $\gamma=\mathcal{O}(\mu)$ and, hence, that $\Psi_1(v)=\mathcal{O}(\mu)$. We expand the exponentials in (38) in μ, retaining only the first-order terms, and set

$$G_1(v^*,v) = \int_{v^*}^{v}\frac{f'(v^-+v)}{g(v)}\,dv,$$
$$G_2(v^*,v) = \int_{v^*}^{v}\frac{f'(v^-+v)}{g(v)}\big(f(v^-+v)-f(v^-)\big)\,dv.$$

Moreover, we neglect the contribution coming from the fast dynamics of (28) and approximate (38) by the corresponding integrals over the two sheets $\mathcal{S}_0^{a\pm}$ of the critical manifold $\mathcal{S}_0$. The relevant v-values are given by v_0 and $v_{\max}$, respectively by $v^*_{\max}$ and 0, as specified in Figure 6; see [1] for details.

Hence, for given w, we find that the leading-order approximation to the corresponding value $\hat{w}$ obtained after one relaxation cycle is given by

$$w\mapsto\hat{w} = \Big(1-\frac{\omega_1\omega_2}{\bar{\omega}^2}\mu\big(G_1(v_0,v_{\max})+G_1(v^*_{\max},0)\big)\Big)w + 2\frac{\omega_1\omega_2}{\bar{\omega}}\Big(\frac{-\gamma+f(v^-)\mu}{\omega_1-\omega_2}\big(G_1(v_0,v_{\max})+G_1(v^*_{\max},0)\big) - \mu\frac{\omega_1-\omega_2}{(\omega_1+\omega_2)^2}\big(G_2(v_0,v_{\max})+G_2(v^*_{\max},0)\big)\Big). \tag{39}$$

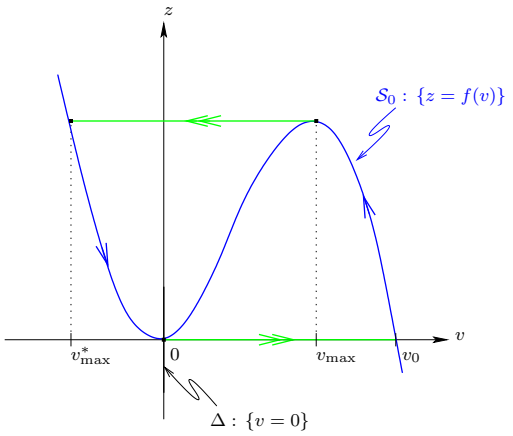

FIG. 6: The geometry of the global return.

The asymptotic formula in (39) describes the global (relaxation) dynamics away from $\ell^{\pm}$ that naturally corresponds to the large-amplitude component ("spiking") of the mixed-mode patterns found in (28).

Next, we recall that these patterns arise via slow passage through a canard explosion at $w=0$ in (28), with the strong canard Γ^0_ε acting as the separatrix between non-trivial mixed-mode behavior (where $w<0$) and the pure relaxation regime, with $w>0$. Hence, for mixed-mode dynamics to be possible, the global return mechanism must generate $\hat{w}<0$ from $w>0$, *i.e.*, the w-independent term in (39) must be negative. More precisely, the critical μ-value μ^c, which marks the onset of pure relaxation in (28) (or, alternatively, the point where non-trivial mixed-mode patterns cease to exist), is defined by the condition

$$\frac{-\gamma+f(v^-)\mu}{\omega_1-\omega_2}\big(G_1(v_0,v_{\max})+G_1(v^*_{\max},0)\big) = \mu\frac{\omega_1-\omega_2}{(\omega_1+\omega_2)^2}\big(G_2(v_0,v_{\max})+G_2(v^*_{\max},0)\big) \tag{40}$$

to leading order. An approximation for μ^c can be obtained by solving (40) for μ. For the parameter values specified in Appendix A, we find $\mu^c\approx 0.1181$ $(0.1063, 0.0988)$ for $\omega_2=16$ $(4, 1.5)$, which is in good agreement with numerical estimates, recall Figures 2 to 4. More importantly, from the form of (40), we deduce that $\mu^c-\frac{\gamma}{f(v^-)}=\mathcal{O}((\omega_2-\omega_1)^2)$, *i.e.*, as $\omega_2\to\omega_1$, the size of the μ-interval over which MMOs are observed in (28) shrinks to 0. This supports the conjecture of [3] that the presence of distal compartments with different diameters (and, hence, varying intrinsic frequencies) underlies the irregular firing that is observed in the dopaminergic neuron *in vivo*.

3.4. The return map Π

To derive the lowest-order description of the return map Π induced by the flow of (30), we proceed as in [1, Section 2], *i.e.*, we divide the phase space of (30) into four distinct regions. We then describe the return map separately in each of these regions, which correspond to

(i) the dynamics in an $\mathcal{O}(\varepsilon^{\frac{1}{4}})$-neighborhood of the fold ℓ^- (Section III **3.2**);

(ii) the entry into this fold region;

(iii) the exit away from the fold;

(iv) and the global relaxation mechanism (Section III **3.3**).

The asymptotic estimates obtained for the return map Π locally in each of the four regions can then be combined into a global, composite formula. The map Π is defined on the (two-dimensional) Poincaré section Δ, which is given by $\{v = 0\}$, cf. again Figure 6, and is most conveniently formulated as a function of $(h, \bar{w})$. Since the analysis of [1] carries over almost verbatim to the context of (30), we will only sketch the argument here; the reader is referred to [1] for details.

The centerpiece of our analysis consists of the asymptotic description of Π close to ℓ^-, see (i); the corresponding local return map will be denoted by $\overline{\Pi}: \ \overline{\Delta}_- \to \overline{\Delta}_-$. To that end, we have to consider a suitably truncated approximation for (30); we first truncate (34c) as follows:

$$\bar{w}' = -2\omega_1\tilde{\mu}\varepsilon^{\frac{5}{4}}\bar{w} + \varepsilon^{\frac{3}{2}}\nu(\tilde{\mu}, 0).$$

Although this approximation is different from the one used in [1, Section 3.3], the following simple observation still enables us to follow closely the development in [1]: A solution $x(t)$ of the linear equation $\dot{x} = ax+b$ with $x(0) = x_0$ is well-approximated by its linearization if $t \in [0, T]$ is such that at is small; namely, $x(t) \approx x_0(1 + at) + bt$. Under the additional (generic) assumption that $h = \mathcal{O}(\varepsilon^M)$ for some $M > 0$, it can be shown that $t \in [0, \mathcal{O}(-\ln\varepsilon)]$ here, see [1] as well as (36); hence, the requirement of at small is equivalent to requiring $\varepsilon^{\frac{5}{4}}\ln\varepsilon$ small, which is certainly the case. Consequently, again in close analogy to [1, Section 3.3], one can show that the following truncation of (34),

$$\begin{aligned}
\bar{v}' &= a(E_2 - v^-)\Big[-\bar{z} + f_2\bar{v}^2 + \varepsilon^{\frac{1}{4}}\Big(f_3 - \frac{f_2}{E_2 - v^-}\Big)\bar{v}^3\Big],\\
\bar{z}' &= \frac{\tilde{\omega}_2}{2}g_{11}\bar{v} + \bar{w}(t),\\
\bar{w}(t) &= \bar{w} - 2\omega_1\tilde{\mu}\varepsilon^{\frac{5}{4}}\bar{w}t + \varepsilon^{\frac{3}{2}}\nu(\tilde{\mu}, 0)t,
\end{aligned} \tag{41}$$

is sufficiently accurate for deriving the lowest-order approximation to $\overline{\Pi}$; a complete justification is beyond the scope of this article. (Here, we have written $\bar{w}(0) = \bar{w}$ now.)

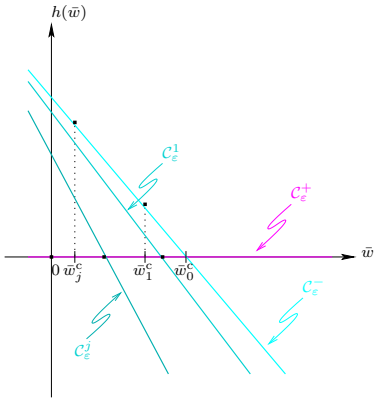

FIG. 7: The curves $\mathcal{C}_\varepsilon^j$ for $j \geq 0$ ($\mathcal{C}_\varepsilon^- \equiv \mathcal{C}_\varepsilon^0$).

Furthermore, the curves $\mathcal{C}_\varepsilon^-$, respectively $\mathcal{C}_\varepsilon^+$, can be defined analogously as in [1], as the intersection of the continuation of $\mathcal{S}_\varepsilon^{a-}$, respectively of $\mathcal{S}_\varepsilon^r$, under the flow of (34) with $\overline{\Delta}$. Similarly, for $j \geq 1$, the curve $\mathcal{C}_\varepsilon^j$ is defined as the image of $\mathcal{C}_\varepsilon^-$ under $\overline{\Pi}^j$, the jth iterate of $\overline{\Pi}$, in $\overline{\Delta}$. As in [1], one finds that for $j \geq 1$, $\mathcal{C}_\varepsilon^j$ can be written as the graph of a function $h^j(\bar{w})$ for $|\bar{w}|$ sufficiently small. Moreover, h^j is approximately linear in $\bar{w}$, see Figure 7.

The global return mechanism in (iv), on the other hand, can to leading order be described by a formula that is obtained from (39) via the rescalings introduced in Section III **3.2**: Given (29) and, in particular, the assumption that $\omega_1 \ll \omega_2$, (39) reduces to the following expression for the global return, which we denote by Π^{ret}:

$$\begin{aligned}
\tilde{w} \mapsto \hat{\tilde{w}} = \Big(1 - 4\frac{\omega_1}{\tilde{\omega}_2}\tilde{\mu}\varepsilon\big(1 + \mathcal{O}(\sqrt{\varepsilon})\big)\\
\times \big(G_1(v_0, v_{\max}) + G_1(v_{\max}^*, 0)\big)\Big)\tilde{w}\\
+ 2\omega_1\tilde{\mu}\varepsilon^{\frac{3}{2}}\Big(\big(\tilde{\gamma} - f(v^-)\tilde{\mu}\big)\big(1 + \mathcal{O}(\sqrt{\varepsilon})\big)\\
\times \big(G_1(v_0, v_{\max}) + G_1(v_{\max}^*, 0)\big)\\
+ \tilde{\mu}\big(1 + \mathcal{O}(\sqrt{\varepsilon})\big)\big(G_2(v_0, v_{\max}) + G_2(v_{\max}^*, 0)\big)\Big);
\end{aligned} \tag{42}$$

see also [1, Equation (2.53)]. Here, the integrals in G_i are again defined as in Section III **3.3**. Recall that (42) describes the dependence of the return point on $\tilde{\mu}$ after one relaxation cycle, and that the pure relaxation regime has been reached if $\hat{\tilde{w}} = \tilde{w}$, *i.e.*, if $\tilde{w}$ is mapped onto itself by the global return so that the small-oscillation regime is bypassed. The associated critical $\tilde{\mu}$-value $\tilde{\mu}^{\mathrm{c}}$ can be estimated by solving

$$\begin{aligned}
\big(\tilde{\gamma} - f(v^-)\tilde{\mu}\big)\big(G_1(v_0, v_{\max}) + G_1(v_{\max}^*, 0)\big)\\
+ \tilde{\mu}\big(G_2(v_0, v_{\max}) + G_2(v_{\max}^*, 0)\big) = 0
\end{aligned}$$

for $\tilde{\mu}$, cf. (40).

Finally, the analysis in the entry and exit regions in (ii) and (iii) can be performed in complete analogy to [1,

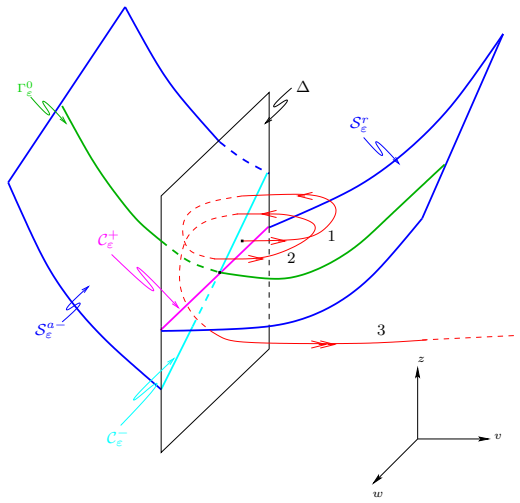

FIG. 8: The generation of mixed-mode dynamics by Π.

Sections 2.3 and 2.4]; the corresponding local maps will be denoted by Π^{in} and Π^{out}, respectively. In sum, the restriction of $\Pi : \Delta \to \Delta$ to the union of the curves $\mathcal{C}_\varepsilon^j$ $(j \geq 1)$ can then be given as follows,

$$\Pi(h^j(\bar{w}), \bar{w}) = \bar{w} + 2\big(\varepsilon^{\frac{3}{2}}\nu(\tilde{\mu}, 0) - 2\omega_1\tilde{\mu}\varepsilon^{\frac{5}{4}}\bar{w}\big)T^{h^j(\bar{w})} + \mathcal{O}(\varepsilon^{\frac{9}{4}}) \quad (43)$$

if $h^j(\bar{w}) > 0$ and

$$\Pi(h^j(\bar{w}), \bar{w}) = \Big(1 - 4\frac{\omega_1}{\tilde{\omega}_2}\tilde{\mu}\varepsilon\Big)\bar{w} + 2\big(\varepsilon^{\frac{3}{2}}\nu(\tilde{\mu}, 0) - 2\omega_1\tilde{\mu}\varepsilon^{\frac{5}{4}}\bar{w}\big) \times T^{h^j(\bar{w}),\text{out}} - \bar{w}\frac{f_2}{\tilde{\omega}_2 g_{11}}\nu(\tilde{\mu}, 0)\varepsilon^{\frac{3}{2}}\ln\varepsilon + \mathcal{O}(\varepsilon^{\frac{5}{4}}) \quad (44)$$

if $h^j(\bar{w}) < 0$. Here, $T^{h^j(\bar{w})}$ is defined as in (36), with h replaced by $h^j(\bar{w})$, and $T^{h^j(\bar{w}),\text{out}} = T^{-h^j(\bar{w})}$.

Finally, we note that the definition of the return map Π depends on the sign of h^j: If $h^j(\bar{w}) > 0$, the point of intersection of the corresponding trajectory of (30) with Δ lies above $\mathcal{C}_\varepsilon^+$. Hence, the trajectory must remain in the fold region (the small-oscillation regime), and the return to Δ is described by the local map $\overline{\Pi}$ in that case. If, on the other hand, $h^j(\bar{w}) < 0$, *i.e.*, if the trajectory intersects Δ below $\mathcal{C}_\varepsilon^+$, it must exit the fold region and undergo a large-amplitude relaxation excursion under the global return. Since, moreover, h^j itself has to be updated after each iteration of Π [1], its sign can change with time, which allows for a transition from small-amplitude "loops" to large-amplitude excursions in (30), or *vice versa*. Hence, in sum, the sign sequence of h^j is in a one-to-one correspondence to the Farey sequence of any given MMO orbit of (30). An exemplary illustration of the above mechanism is given in Figure 8, which shows how the symbolic segment 1^2 is generated by iterating Π.

3.5. Secondary canards and sectors of rotation

The so-called jth secondary canard Γ_ε^j is defined [1] as a trajectory that undergoes j small (non-relaxation) rotations, or "loops," in the fold region before entering relaxation. Then, the values of $\bar{w}$ in $\mathcal{C}_\varepsilon^-$ that correspond to Γ_ε^j are determined by finding the points of intersection of subsequent iterates of $\mathcal{C}_\varepsilon^-$ under $\overline{\Pi}$ with $\mathcal{C}_\varepsilon^+$. These $\bar{w}$-values will be denoted by $\bar{w}_j^{\text{c}}$ $(j \geq 0)$, *i.e.*, the point of intersection of $\mathcal{C}_\varepsilon^j$ with $\mathcal{C}_\varepsilon^+$ is precisely the image of $\bar{w}_j^{\text{c}}$ under $\overline{\Pi}^j$; see again Figure 7. The jth *sector of rotation* RS^j is then defined as the subinterval $(\bar{w}_j^{\text{c}}, \bar{w}_{j-1}^{\text{c}}) \subset \mathcal{C}_\varepsilon^-$, cf. Figure 9; this definition can be extended into a neighborhood of $\mathcal{C}_\varepsilon^-$ by the flow of (34).

The strong canard Γ_ε^0, with $j = 0$, is obtained in the intersection of $\mathcal{C}_\varepsilon^-$ and $\mathcal{C}_\varepsilon^+$, *i.e.*, under the zeroth iterate of $\overline{\Pi}$. It can be shown as in [1, 22] that the corresponding $\bar{w}$-value $\bar{w}_0^{\text{c}}$ is to lowest order determined by solving the condition $d_{\bar{w}}^0\bar{w} + d_\varepsilon^0\varepsilon^{\frac{1}{4}} = 0$ for $\bar{w}$. Here, the coefficients $d_{\bar{w}}^0$ and d_ε^0 are given by

$$d_\varepsilon^0 = \int_{-\infty}^{\infty} \nabla H(\bar{\gamma}_0^0(t)) \cdot \big(a((E_2 - v^-)f_3 - f_2)\bar{v}_0^0(t)^3 + a\bar{v}_0^0(t)\bar{z}_0^0(t), g_{12}\bar{v}_0^0(t)^2\big)^T dt, \quad (45a)$$

$$d_{\bar{w}}^0 = \int_{-\infty}^{\infty} \nabla H(\bar{\gamma}_0^0(t)) \cdot (0, 1)^T dt, \quad (45b)$$

cf. also [1, Proposition 2.2], with H and $\bar{\gamma}_0^0$ defined as above and g_{12} the second-order coefficient in the expansion of $g_1(v)(E_1 - v)$ about v^-. The integrals in (45) can be evaluated exactly [1, 22]; in particular, it follows that

$$\bar{w}_0^{\text{c}} = -\frac{d_\varepsilon^0}{d_{\bar{w}}^0}\varepsilon^{\frac{1}{4}} + \mathcal{O}(\varepsilon^{\frac{1}{2}}). \quad (46)$$

Similarly, to determine the $\bar{w}$-value $\bar{w}_1^{\text{c}}$ corresponding to the first secondary canard Γ_ε^1, we have to find the point of intersection of $\mathcal{C}_\varepsilon^1$ with $\mathcal{C}_\varepsilon^+$. As it turns out, the corresponding defining condition for $\bar{w}_1^{\text{c}}$ derived in [1, Equation (3.21)] will now have the form

$$P_h\overline{\Pi}_0(h^0(\bar{w}), \bar{w}) = -\big(\varepsilon^{\frac{3}{2}}\nu(\tilde{\mu}, 0) - 2\omega_1\tilde{\mu}\varepsilon^{\frac{5}{4}}\bar{w}\big)\mathcal{K}(h^0(\bar{w})) + \mathcal{O}(\varepsilon^{\frac{9}{4}}). \quad (47)$$

Here, h^0 is the value of h corresponding to $\bar{w} \in \mathcal{C}_\varepsilon^-$, P_h denotes the projection onto the h-coordinate, and $\overline{\Pi}_0$ is the transition map for the simplified truncated system that is obtained for $\bar{w}(t) \equiv \bar{w}$ constant in (41). By way of an analogous computation as in [1], it can be shown that $\mathcal{K}(h) = 2d_{\bar{w}}^0 T^h + \mathcal{O}(1)$, where $d_{\bar{w}}^0$ is defined in (45b).

Then, proceeding as in the proof of Proposition 3.2 in [1], we find

$$\bar{w}_1^{\text{c}} = \bar{w}_0^{\text{c}} - 2\big(\varepsilon^{\frac{3}{2}}\nu(\tilde{\mu}, 0) - 2\omega_1\tilde{\mu}\varepsilon^{\frac{5}{4}}\bar{w}_0^{\text{c}}\big)T^{h(\bar{w}_1^{\text{c}})} + \mathcal{O}(\varepsilon^{\frac{9}{4}}), \quad (48)$$

or, by combining (46) and (48),

$$\bar{w}_1^{\mathrm{c}} = \bar{w}_0^{\mathrm{c}} - 2\varepsilon^{\frac{3}{2}}\Big(\nu(\tilde{\mu},0) + 2\omega_1\tilde{\mu}\frac{d_\varepsilon^0}{d_{\bar{w}}^0}\Big)T^{h(\bar{w}_1^{\mathrm{c}})} + \mathcal{O}(\varepsilon^{\frac{7}{4}}). \tag{49}$$

Now, from an a posteriori argument as in [1, Section 3.3], it follows that $h^j(\bar{w}_1^{\mathrm{c}}) = \mathcal{O}(\varepsilon^{\frac{3}{2}}\sqrt{-\ln\varepsilon})$, which, together with (36), implies that the lowest-order approximation for the sector width $\Delta\bar{w} := \bar{w}_1^{\mathrm{c}} - \bar{w}_0^{\mathrm{c}}$ is given by

$$\Delta\bar{w} = -\frac{2\sqrt{6}\big(\nu(\tilde{\mu},0) + 2\omega_1\tilde{\mu}\frac{d_\varepsilon^0}{d_{\bar{w}}^0}\big)}{\sqrt{a(E_2-v^-)\tilde{\omega}_2 g_{11}}}\varepsilon^{\frac{3}{2}}\sqrt{-\ln\varepsilon}.$$

Therefore, $\Delta\bar{w} = \mathcal{O}(\varepsilon^{\frac{3}{2}}\sqrt{-\ln\varepsilon})$; moreover, it can be shown as in [1] that the size of all rotation sectors will be the same to leading order, *i.e.*, that $\bar{w}_j^{\mathrm{c}} - \bar{w}_{j-1}^{\mathrm{c}} = \mathcal{O}(\varepsilon^{\frac{3}{2}}\sqrt{-\ln\varepsilon})$ for any $j \geq 1$. Finally, since $\Delta\bar{w} < 0$, it follows that the sector RS^j will lie the closer to Γ_ε^0 the smaller j is; cf. Figure 9.

3.6. The reduced return map Φ

The final step in the analysis of the mixed-mode dynamics of (30) consists in a reduction of the two-dimensional return map Π, which is a priori defined on $\cup\mathcal{C}_\varepsilon^j$, to a simplified, one-dimensional map $\Phi : \mathcal{C}_\varepsilon^- \to \mathcal{C}_\varepsilon^-$, with

$$\Phi(\bar{w}) = P_{\bar{w}}\big(\Pi^{\mathrm{in}} \circ \Pi^{\mathrm{ret}} \circ \Pi^{\mathrm{out}} \circ \overline{\Pi}^k(h^0(\bar{w}),\bar{w})\big)$$

if $(h^0(\bar{w}),\bar{w}) \in RS^k$. (Here, $P_{\bar{w}}$ denotes the projection onto the $\bar{w}$-coordinate.) The main advantage of this reduction lies in the fact that it reduces the description of the flow induced by (30) to the analysis of a one-dimensional map that is defined on the single curve $\mathcal{C}_\varepsilon^-$. Moreover, Φ is unimodal on each of the sectors of rotation RS^k and can hence be analyzed using standard techniques. Detailed results on the dynamics of Φ have been derived in [1, Section 3]. All these results can be generalized in a straightforward manner, and adapted to the present context; again, the only difference lies in the powers of ε that will occur. In this subsection, we rederive some of the properties of Φ in the framework of (30). A qualitative illustration of Φ can be found in Figure 9.

One important quantity for our analysis is given by the derivative of Φ with respect to $\bar{w}$ on RS^k, since it allows us to estimate the contraction, or expansion, of the dynamics under Φ. As in [1, Lemma 3.5], it follows with (31) that

$$\Phi'(\bar{w}) := \frac{d\Phi(\bar{w})}{d\bar{w}} = 1 + \varepsilon^{\frac{3}{2}}\Big(\nu(\tilde{\mu},0) + 2\omega_1\tilde{\mu}\frac{d_\varepsilon^0}{d_{\bar{w}}^0}\Big) \times \left(\sum_{j=0}^{k-1} 2\frac{dT^{h^j(\bar{w})}}{d\bar{w}} + \frac{dT^{h^k(\bar{w}),\mathrm{out}}}{d\bar{w}}\right) + \mathcal{O}(\varepsilon^{\frac{5}{4}}\sqrt{-\ln\varepsilon}).$$

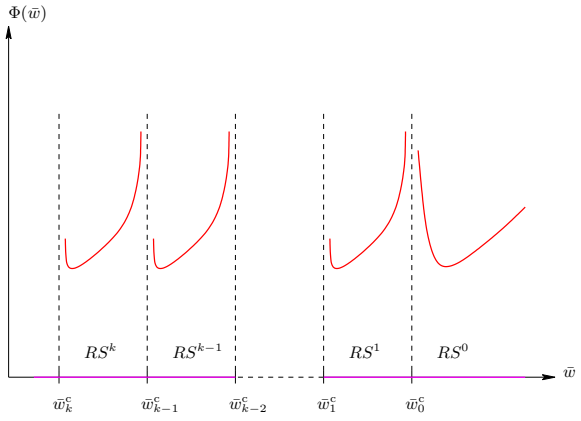

FIG. 9: The reduced return map Φ.

Arguing as in [1, Section 3.5] and taking into account (36), we find

$$\Phi'(\bar{w}) = 1 - \varepsilon^{\frac{3}{2}}\frac{\nu(\tilde{\mu},0)d_{\bar{w}}^0 + 2\omega_1\tilde{\mu}d_\varepsilon^0}{\sqrt{a(E_2-v^-)\tilde{\omega}_2 g_{11}}} \times \left(\sum_{j=0}^{k-1} 2(j+1)\frac{1}{h^j(\bar{w}^j)}\frac{1}{\sqrt{-\ln h^j(\bar{w}^j)}} + (k+1)\frac{1}{h^k(\bar{w}^k)}\frac{1}{\sqrt{-\ln h^k(\bar{w}^k)}}\right) + \mathcal{O}(\varepsilon^{\frac{5}{4}}\sqrt{-\ln\varepsilon}). \tag{50}$$

Then, making again use of $h^j(\bar{w}^j) = \mathcal{O}(\varepsilon^{\frac{3}{2}}\sqrt{-\ln\varepsilon})$, we can write

$$\frac{1}{\sqrt{-\ln h^j(\bar{w}^j)}} = \frac{\sqrt{2}}{\sqrt{-3\ln\varepsilon}}\big(1 + o(1)\big)$$

and, hence,

$$\Phi'(\bar{w}) \sim 1 - \frac{\nu(\tilde{\mu},0)d_{\bar{w}}^0 + 2\omega_1\tilde{\mu}d_\varepsilon^0}{\sqrt{a(E_2-v^-)\tilde{\omega}_2 g_{11}}}\frac{\sqrt{2}\varepsilon^{\frac{3}{2}}}{\sqrt{-3\ln\varepsilon}} \times \left(\sum_{j=0}^{k-1}\frac{2(j+1)}{h^j(\bar{w}^j)} + \frac{k+1}{h^k(\bar{w}^k)}\right).$$

Finally, using a combination of (49) and an argument analogous to the one preceding [1, Equation (3.33)], we obtain

$$\Phi'(\bar{w}) \sim 1 - \frac{\omega_k(\eta)}{6\ln\varepsilon}, \tag{51}$$

where the function ω_k is defined via

$$\omega_k(\eta) = \sum_{j=0}^{k-1}\frac{1}{(k-j)-\eta} - \frac{1}{2\eta}.$$

Here, $\eta > 0$ for $k = 0$ and $\eta \in [0,1]$ for $k \geq 1$, respectively.

In the following, we summarize some of the main findings of [1] in the framework of (30). Given that the qualitative dynamics of Φ is exactly as derived in [1, Section 3.6], the corresponding proofs carry over almost unchanged; hence, we omit them here.

The first important result in [1] concerns the existence and stability of periodic MMO orbits of the type 1^k, *i.e.*, of orbits undergoing one large (relaxation) excursion followed by k small (non-relaxation) loops. In analogy to [1, Theorem 3.7], one can show that these orbits will exist and be stable on a $\tilde{\mu}$-interval whose width is to leading order given by

$$\Delta\tilde{\mu}^k = \mathcal{O}\big(\varepsilon^{\frac{1}{4}}(-\ln\varepsilon)^{-\frac{1}{2}}\big) \tag{52}$$

for ε sufficiently small. The proof of (52) is based on deriving a sufficient condition for $|\Phi'| < 1$ in dependence on $\tilde{\mu}$, taking into account that

$$\frac{d\tilde{\mu}}{d\bar{w}} = -\frac{\frac{\partial\Phi}{\partial\bar{w}} - 1}{\frac{\partial\Phi}{\partial\mu}} \sim \frac{\omega_k(\nu)}{6D_{\tilde{\mu}}\varepsilon^{\frac{5}{4}}\ln\varepsilon} \tag{53}$$

by (42) and (51); here, $D_{\tilde{\mu}}$ denotes the $\tilde{\mu}$-derivative of the right-hand side in (42), cf. [1, Section 2.5]. Then, integrating (53) with respect to η and applying the Fundamental Theorem of Calculus, one obtains (52). Note that (52) in particular implies that the corresponding μ-interval will be of the order $\mathcal{O}(\varepsilon^{\frac{3}{4}}(-\ln\varepsilon)^{-\frac{1}{2}})$, recall $\mu = \sqrt{\varepsilon}\tilde{\mu}$.

Given (52), it can be shown that Theorems 3.9 and 3.10 from [1] carry over almost verbatim into the context of (30). Recall the definition of the Farey sequence $\{L_j^{k_j}\}$ that is associated to the MMO orbit in (30) consisting of $L_j \geq 1$ relaxation excursions and $k_j \geq 1$ small (non-relaxation) oscillations. Then, we conclude as in [1] that, "generically,"

1. for $L_j = 1$, orbits must consist of segments of the form 1^k (some number of times in succession), 1^{k-1} (some number of times in succession), and 1^{k-2} preceded by 1^k and followed by 1^{k-1} or 1^k;
2. for $L_j = 2$, only segments of the type 2^1 or 2^2 will occur;
3. for $L_j \geq 3$, only segments of the form L_j^1 will be observed.

These predictions are confirmed by numerical simulations that are presented in Section IV below.

IV. DISCUSSION

In this article, we have analyzed a slightly simplified version of the so-called Wilson-Callaway model [3, 5] from a geometric point of view. We have shown how the model equations that were proposed in the two-compartment case in [4] can be fitted into the framework of [1]. The only real difference between the detailed asymptotics obtained for (5) in [1] and the formulae derived here lies in the fact that the powers of ε that occur, as well as their respective ratios, are slightly different. Yet, the basic features of the two systems–the three time-scale structure and the presence of a folded saddle-node singularity as well as of one natural bifurcation parameter, say–are the same. Consequently, our results in both cases are qualitatively identical as far as the resulting mixed-mode dynamics is concerned, see Section III **3.6**. In other words, although the asymptotics obtained here are quantitatively different from those in [1], the techniques used in the analysis are very similar. There is of course potential for a more thorough investigation than outlined here; in particular, we emphasize that all the coefficients occurring in our formulae are computable, in the sense that their numerical values are completely determined by the choice of parameters in (3), as, *e.g.*, in Appendix A.

Since the present study is largely mathematical, rather than mechanistic, it might be too speculative to try and apply our findings directly to the original, physiological Wilson-Callaway model [3]. However, two remarks are still in order: First, the bifurcation mechanism, physiologically speaking, is regulated by the rate of calcium efflux from the neuron, which corresponds precisely to the control parameter τ. Upon variation of τ, one can observe varying numbers of subthreshold oscillations. For τ large enough, the oscillatory dynamics breaks down, in agreement with the findings of [3], where voltage-gated calcium currents are identified as being essential for sustaining the oscillation.

Second, it is worth pointing out that the results of Section III are based on the assumption that the intrinsic frequencies of adjacent neuronal compartments are vastly different, *i.e.*, that $\omega_1 \ll \omega_2$ in our case. If this condition is not satisfied, our analysis of the passage through the fold region is no longer valid. The necessary tools for a more complete analysis are still being developed [9]. One result we have obtained here is an approximation for the global return mechanism irrespective of the sizes of ω_i, as well as an estimate of the μ-interval on which MMOs exist in (3); cf. equation (40). This estimate leads to the interesting conclusion that the relevant μ-range shrinks to zero as $\omega_2 \to \omega_1$, which can be interpreted physiologically as follows: Studied *in vivo*, the dopaminergic neuron displays three types of oscillatory behavior, regular firing, irregular firing, and bursting [3]. If MMOs were related to irregular firing sequences, the fact that they vanish for $\omega_2 \to \omega_1$ would corroborate the conjecture of [3] that the presence of distal compartments with significantly different natural frequencies is the cause of irregular firing.

From a mathematical point of view, one principal result of our analysis is the accurate reduction of the global return map Π, which is defined as a two-dimensional map on the Poincaré section Δ, to a one-dimensional map Φ. The map Φ is defined on a *set of intervals* (each corresponding to a sector of rotation), approximates Π with an

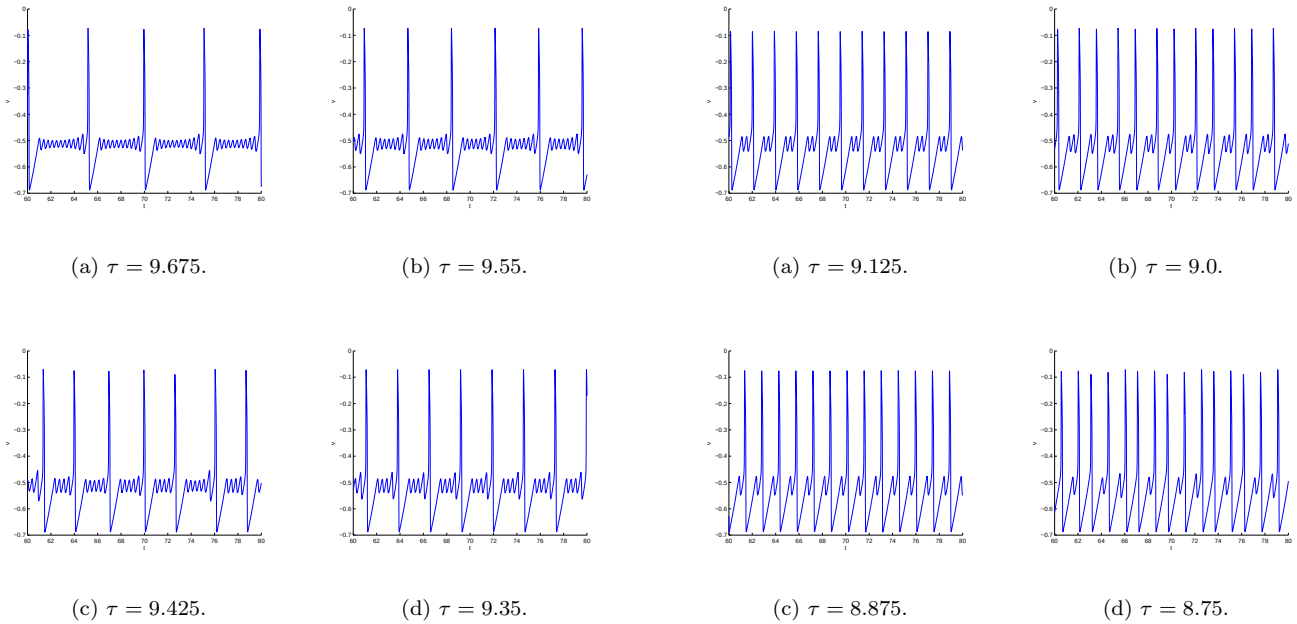

(a) $\tau = 9.675$. (b) $\tau = 9.55$. (c) $\tau = 9.425$. (d) $\tau = 9.35$.

FIG. 10: Time series of v in (21): As τ decreases, one observes a transition from (a) $1^{11}1^{10}$ via (b) 1^7 and (c) $1^61^51^4$ to (d) 1^4 in the resulting Farey sequences.

(a) $\tau = 9.125$. (b) $\tau = 9.0$. (c) $\tau = 8.875$. (d) $\tau = 8.75$. (e) $\tau = 8.625$. (f) $\tau = 8.5$.

FIG. 11: Time series of v in (21): As τ decreases, one observes a transition from (a) 1^2 via (b) 1^21^1, (c) 1^1, (d) 2^11^1, and (e) 3^1 to (f) 1^0 in the resulting Farey sequences.

only exponentially small error (in ε), and can be studied using standard techniques.

On the other hand, our analysis also shows that a straightforward reduction of Π to a one-dimensional map defined on a *single* interval is not possible, as postulated by some authors [4, 6]. More precisely, the analysis of [4] does not resolve the canard structure of system (3) in detail; rather, the Hopf and canard points are "lumped" together into a single point, and this simplification is employed to formulate a piecewise linear return map for (3) that is a function of K. Our analysis, on the other hand, resolves the structure between the Hopf point and the canard point in detail. In particular, we show that there exists an entire family of secondary canards in between these points, and that these canards correspond in a unique fashion to the number of small-amplitude "loops" observed in a given MMO trajectory of (3), in that they bound the corresponding sectors of rotation. Moreover, the asymptotics of this map Φ can be described in detail to make precise qualitative and quantitative predictions on the admissible Farey sequences, whereas a generic piecewise linear map will allow for a much wider range of possible sequences to occur.

Some of our principal findings from [1] can be translated into the context of the transformed (v, z, w)-system (21) (and, consequently, of the original equations in (3)) as follows; details can be found in [1]:

1. Sequences of the form $\{1^k\}$ and $\{1^k1^{k-1}\}$ dominate the stable dynamics; these sequences correspond to MMO trajectories that visit only one sector, respectively two adjacent sectors.

2. Segments of the form $L_j^{k_j}$ with $L_j \geq 2$ are not observed when $k_j \geq 2$, except for the segment 2^2. The segment L_j^1, however, is admissible for any $L_j \geq 1$.

3. As μ increases, the sequences observed in the transition are roughly of the form $\ldots \to 1^k \to 1^k1^{k-1} \to 1^{k-1} \to \ldots$, implying that the dynamics "sweeps through" all sectors of rotation before entering the relaxation regime for $\mu > \mu^c$.

4. The local dynamics depends quite sensitively on the curvature of $f(v)$, *i.e.*, on f_2, in the sense that 1^k-type orbits become increasingly harder to observe as f_2 increases.

5. The number of sectors visited also depends on the strength of the global dynamics, *i.e.*, on how far w is reset after relaxation; by (42), the corresponding

return point will typically be $\mathcal{O}(\varepsilon^{\frac{3}{2}})$-close to the strong canard Γ^0_ε.

6. The sector width is given by $\Delta\bar{w} = \mathcal{O}(\varepsilon^{\frac{3}{2}}\sqrt{-\ln\varepsilon})$ to leading order, which implies that the global return point will in general lie in one of the lower sectors of rotation, by 5. Hence, one tends to observe a sub-maximum number of small oscillations.

7. The sector size decreases as k increases or, equivalently, as μ decreases; however, we conjecture that the overall dynamics becomes less expanding with higher k, making it less likely for segments of the form $1^k1^{k-\ell}$, $\ell > 1$, to occur.

With the exception of the conjecture in 7., these observations are reflected by our numerical findings, cf. Figures 10 and 11, and are in excellent agreement with the numerical results obtained in [4], see in particular their Figure 3. All numerical simulations were performed in MATLAB using the predefined routine `ode15s` with absolute and relative accuracies 10^{-10} and 10^{-8}, respectively. For clarity, the results are illustrated starting at $t = 60$, after initial transients have subsided.

Acknowledgments

The authors are grateful to Jaime Cisternas, Alexey Kuznetsov, Georgi Medvedev, Björn Sandstede, and Martin Wechselberger for valuable discussions and comments. The research of M.K. was supported in part by NSF grant DMS-0406608. The research of N.P. was supported by NSF grants DMS-0109427 (to N.K.), DMS-0211505 (to N.K.), and DMS-0406608 (to M.K.). The research of N.K. was supported in part by NSF grant DMS-0211505.

APPENDIX A: PARAMETER VALUES

The parameter values used throughout this article are as follows:

$$E_1 = 1.0,\ E_2 = -0.9,\ E_3 = -0.5,$$
$$\bar{g}_1 = 0.8,\ \bar{g}_2 = 2.0,\ \bar{g}_3 = 1.0,$$
$$c_1 = -0.35,\ c_2 = 0.07,\ c_3 = 1.8,$$
$$\omega_1 = 1.0,\ \omega_2 = 16.0,\ \tau = 10.0,\ d = 4444,\ \varepsilon = 0.013.$$

The linearization of $g_2(u_i)$ about $u_i = 2$ is given by $g_2(u_i) \approx -au_i + b$, where the coefficients a and b are fitted to $a = -0.9569$ and $b = -0.7241$, respectively.

***Remark* 5.** Note that the value of c_2 differs from the one cited in [4, Appendix A]; in fact, we did not succeed in obtaining MMOs numerically using the c_2-value from [4].

[1] M. Krupa, N. Popović, and N. Kopell (2007), submitted to SIAM J. Appl. Dyn. Syst.

[2] Y. L. Li, R. Bertram, and J. Rinzel, Neuroscience **71**, 397 (1996).

[3] C. J. Wilson and J. C. Callaway, J. Neurophysiol. **83**, 3084 (2000).

[4] G. S. Medvedev and J. E. Cisternas, Physica D **194**, 333 (2004).

[5] G. S. Medvedev, C. J. Wilson, J. C. Callaway, and N. Kopell, J. Comp. Neurosci. **15**, 53 (2003).

[6] A. Milik, P. Szmolyan, H. Löffelmann, and E. Gröller, Int. J. Bif. Chaos **8**, 505 (1998).

[7] M. Brøns, M. Krupa, and M. Wechselberger, Fields Inst. Comm. **49**, 39 (2006).

[8] A. Milik and P. Szmolyan, in *Multiple-time-scale dynamical systems*, edited by C. K. R. T. Jones and A. I. Khibnik (Springer-Verlag, New York, 2001), vol. 122 of *IMA Vol. Math. Appl.*, pp. 117–140.

[9] M. Brøns, M. Krupa, and M. Wechselberger (2007), in preparation.

[10] M. Wechselberger, SIAM J. Appl. Dyn. Syst. **4**, 101 (2005).

[11] J. Rubin and M. Wechselberger (2007), to appear in Biol. Cybernet.

[12] J. Moehlis, J. Nonlinear Sci. **12**, 319 (2002).

[13] G. S. Medvedev and N. Kopell, SIAM J. Appl. Math. **61**, 1762 (2001).

[14] N. Fenichel, J. Differential Equations **31**, 53 (1979).

[15] E. Benoit, J.-L. Callot, F. Diener, and M. Diener, Collect. Math. **31**, 37 (1981).

[16] F. Dumortier, in *Bifurcations and Periodic Orbits of Vector Fields*, edited by D. Schlomiuk (Kluwer Academic Publishers, Dordrecht, 1993), no. 408 in NATO ASI Series C, Mathematical and Physical Sciences, pp. 19–73.

[17] F. Dumortier and R. Roussarie, Mem. Amer. Math. Soc. **121** (1996).

[18] W. Eckhaus, in *Asymptotic Analysis, II* (Springer-Verlag, Berlin, 1983), vol. 985 of *Lecture Notes in Math.*, pp. 449–494.

[19] P. Szmolyan and M. Wechselberger, J. Differential Equations **177**, 419 (2001).

[20] B. Sandstede, personal communication.

[21] J. Jalics, M. Krupa, H. G. Rotstein, and N. Kopell (2007), to appear in Chaos.

[22] M. Krupa and P. Szmolyan, J. Differential Equations **174**, 312 (2001).